21PM2A-01

Progress in Microwave Imaging of Plasmas and Applications

A. Mase[#1], N. Ito[#2], Y. Kogi[*3], H. Ikezi[#4], M. Inutake[##5], X. Wang[#6], D. Kuwahara[**7], Y. Nagayama[**8], T. Yoshinaga[**9], S. Yamaguchi[###10], S. K. Padhi[***11]

[#] *Art, Science and Technology Center for Cooperative Research, Kyushu University, Kasuga 816-8580, Japan*

[1] mase@astec.kyushu-u.ac.jp

[2] itonao3@astec.kyushu-u.ac.jp

[4] ikezi7249@sbcglobal.net

[6] wang@astec.kyushu-u.ac.jp

[*] *Fukuoka Institute of Technology, Fukuoka 811-0295, Japan*

[3] kogi@fit.ac.jp

[##] *Research Institute of Electrical Communication, Tohoku University, Sendai 980-8577, Japan*

[5] inutakem@riec.tohoku.ac.jp

[**] *National Institute for Fusion Science, Toki 509-5292, Japan*

[7] dkuwahar@cc.tuat.ac.jp

[8] nagayama.yoshio@nifs.ac.jp

[9] yoshinag@nda.ac.jp

[###] *Faculty of Engineering Science, Kansai University, Suita 564-8680, Japan*

[10] yamso16@kansai-u.ac.jp

[***] *International Centre for Radio Astronomy Research, Curtin University, Perth, WA 6845, Australia*

[11] S.Padhi@curtin.edu.au

Abstract—**Progress in micro- to millimeter-wave technologies have made possible advanced diagnostics (imaging) for various applications, such as, plasma diagnostics, radio astronomy, alien substance detection, airborne and spaceborne imaging radars called as synthetic aperture radars, living body measurements. In this report we focus on the reflectometric (radar) techniques applied to plasma diagnostics and biomedical measurement.**

I. INTRODUCTION

Reflectometry has been used to measure plasma density/ temperature profiles and their fluctuations [1]. When an electromagnetic wave is launched into a plasma, the wave is reflected at the corresponding cutoff layer. Due to high localization of measurements, noninvasive nature and low requirements to an access port window, reflectometry has become an ordinary diagnostics, and it is now utilized on a number of magnetic fusion devices.

In microwave reflectometry, the WKB approximation is often used for interpretation of the received signal. According to this approximation, plasma fluctuations are supposed to affect phase of a probing signal and do not change its amplitude. Therefore, near the cutoff region the shape of the signal wavefront corresponds to the shape of the fluctuations. If the amplitude of the fluctuations is small or the width of their wavenumber spectrum is narrow, the microwaves bear phase information on a large distance and interpretation of the signal is straightforward. Otherwise, interference of the scattered wavefronts destructs the shape of phase close to the cutoff position making difficult extraction of the information from the reflectometer signal. One of the possible ways to solve this problem is microwave imaging reflectometry (MIR) [2-4] using large aperture optics to restore the wavefronts at the receiver position. The MIR concept is valid until the cutoff can be considered as the phase-screen.

In industrial applications, microwave imaging of the complex permittivity profile of an unknown object buried under dielectric interface or half-space is an important technology that has been used successfully in subsurface sensing such as Ground Penetrating Radar (GPR) [5]. Other potential applications include nondestructive testing of materials, biomedical imaging, [6, 7] and the detection of defects and cracks in construction materials [8]. Recently, the approach has received considerable attention due to its potential advantages over more established techniques, such as X-ray tomography, as an alternative tool in medical diagnostics, the detection of breast cancers. Today breast cancer is the most common form of cancer among women, and the standard method of diagnosing breast cancer, is by X-ray mammography. Despite its wide-scale usage, there is a limit in detection sensitivity, since the contrast of dielectric constant between malignant and normal breast tissues is small in the X-ray frequencies comparing to that in microwave frequencies. These limitations provide clear motivations for investigation for alternate or complimentary diagnostic

In general, two different approaches are used to detect the dielectric contrast between the object and the background medium: radar-type backscattering methods and tomographic methods. In the radar-type methods, an ultra-wideband signal

illuminates the object from several directions and the amplitude and the arrival time of the reflected signals are used to identify the location of the strong scatterer. In the tomographic approach, the measured scattering data is used to recover quantitative images of the dielectric profile using either linear or non-linear approximations. Linear techniques such as Born and Rytov approximations have been used widely in the image reconstruction process for weak scatterers as first order approximation [9]. However, for large objects with high contrast ratio, such as often found in biological tissue structures, iterative nonlinear methods are used which usually involve the minimization of cost function. This paper focuses on radar-type method for breast imaging.

II. Microwave Imaging in Plasma Diagnostics

In this section is described the development of a millimetre-wave imaging system applied to the large helical device (LHD) in National Institute for Fusion Science, Japan.

A. Experimental Arrangement

A combined system of MIR and ECEI (electron cyclotron emission imaging) as shown in Fig. 1 has been applied to the Large Helical Device (LHD) [4]. The MIR system uses 4 different frequency sources in order to obtain the information at 4 radial positions. The frequencies at 750, 983, 1183 and 1450 MHz from the crystal oscillators are separately up-converted with the 18.33 MHz from the crystal oscillator. These frequencies are mixed with the carrier frequency at 9.3 GHz from a voltage-controlled-oscillator (VCO). Upper side-band frequency components at 10.068, 10.301, 10.501 and 10.768 GHz are utilized. The bandpass filters (BPFs) drop lower side-band components to lower than -40dB. The 4 frequencies are separately sextupled, and combined by directional couplers. The output signal with frequencies of 60.410, 61.808, 63.008 and 64.610 GHz is then amplified and irradiated to a target plasma as a probing beam.

In the early stage of experiment, reflected waves from the cutoff surfaces corresponding to each frequency are focused via the imaging optics onto an aperture of 2-D horn antenna array (HAA) with mixers. The array consists of 35 small horns aligned in toroidally 5 by poloidally 7 channels. The received wave is mixed with the first-LO signal at 55.800 GHz by Schottky diode mixers. The frequency is obtained by sextupling 9.300 GHz from a VCO. The down-converted first-by Schottky diode mixers. The frequency is obtained by sextupling 9.300 GHz from a VCO. The down-converted first-

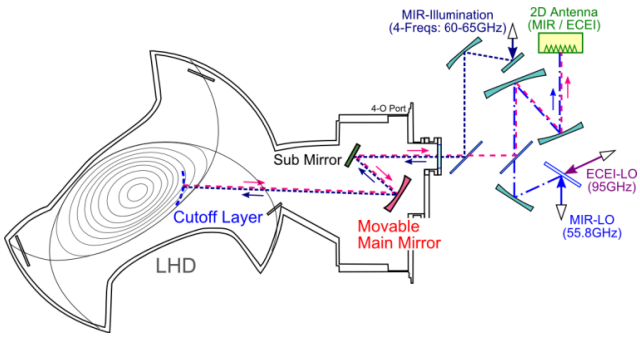

Fig. 1. Microwave imaging system on LHD.

sextupling 9.300 GHz from a VCO. The down-converted first-IF signal (RF-LO) consists of 4 frequency components at 4.610, 6.008, 7.208 and 8.810 GHz. These first-IF frequency components are separated by a BPF bank fabricated by microwave integrated circuit (MIC) technology. The separated first-IF signals are down-converted again by mixing with 4 second-LO signals (4.500, 5.898, 7.098 and 8.700 GHz). The second-IF signals all at 110 MHz are finally obtained for the amplitude and phase detection by the power detector and the quadrature-demodulator. Recently, a 2-D horn-antenna mixer array (HMA) is developed instead of HAA, which consists of arrayed quasi-optical antenna-mixers covered with pyramidal horn apertures.

The ellipsoidal or hyperboloidal surfaces of the curved aluminum alloy mirrors were determined for simultaneous focusing of the above three wave components (the illuminating waves, the reflected waves, and the first LO wave). The focusing optics of the reflected waves on the HMA aperture and the illuminating optics for probe waves were designed first to match the existing movable main mirror. The LO wave transmission optics was matched to the previously designed mirror so that the LO beam covers the whole aperture area with a 100mm×100mm rectangle to supply enough power for down-conversion (−16 dBm) to the mixer diodes. The optics is designed by using the 2-D finite-difference time-domain (FDTD) method. Since the numerical solutions of the Maxwell equations are directly computed in the FDTD calculation, the effect of finite wavelength can be intrinsically simulated. An adjustable ellipsoidal mirror is installed in the vacuum chamber in order to control the illumination angle. The mirror angles are remotely controlled by non-magnetic actuators with ultrasonic motors as shown in Fig. 1. Separation between the illumination and the detection optics reduces the back ground noise due to the stray wave. Note that the adjustment of the mirror angle is extremely important for the LHD experiment, since the optimum angle is changed in 1 degree.

B. MIR Signal from Plasmas

Figure 2 shows typical waveforms of the MIR signals. The fluctuating signals in both amplitude and phases are excited during the period of finite electron density. This suggests that the present MIR system can achieve those fluctuation signals from the plasma itself rather than from the electron-cyclotron heating (ECH) pulses or the neutral-beam injection (NBI). The fast Fourier transform (FFT) spectra of the MIR signals accompany equally-spaced higher order harmonics. The components with the fundamental and the second harmonic frequency at several kHz can be found also in the magnetic fluctuation's spectrum. This also supports that the MIR system is indeed observing the plasma. Meanwhile, the higher order harmonics can only be seen in the MIR signals, The frequency of the oscillation seems to vary as increasing of electron density. Since present MIR uses X-mode cutoff, the observation area corresponds to the magnetic field strength as well as the electron density. The first result of 3-D image of the MHD instability shows that a localized fluctuation burst is observed on the edge plasma in LHD.

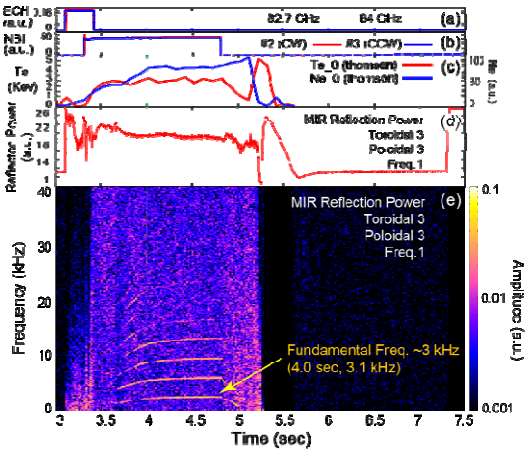

Fig. 2. Experimental result: (a) ECH timing, (b) NBI timing, (c) electron temperature and density, (d) MIR signal (60.41 GHz), (e) FFT spectra of (d).

III. Microwave Imaging for Breast Cancer Detection

In this paper, the experiments of breast cancer detection using an ultrashort-pulse radar (USPR) with a compact vivaldi antenna are described. The antenna has a wide bandwidth ranging from 3 GHz to 12 GHz. An impulse with no distortion can be utilized as an incident wave for two-dimensional study to perform the image reconstruction.

A. Numerical Simulation

In numerical simulations, we solve Maxwell's equations describing the propagation of electromagnetic wave and its scattering and reflection by an object based on the FDTD model. A foreign object having a permittivity different from an object to be inspected causes wave reflection and scattering. Breast has rather simple structure and lower dielectric constant and loss tangent than the other part of human body. In addition, the dielectric properties of breast tumors are much higher than the normal breast tissue. We assume that the dielectric property of normal breast tissue is $\varepsilon_r = 9$, $\sigma = 0.4$ S/m and that of the malignant breast tissue is $\varepsilon_r = 50$, $\sigma = 4$ S/m [7]. A Gaussian-shape pulse with a 65 ps full-width half-maximum (FWHM) is irradiated to the breast through an antenna located at the position of 10 cm apart from the breast surface. The antenna is rotated every 10 degree around the breast from 0 to 180 degrees. The reflected waves from the skin and the tumor are received by the identical antenna.

The reconstruction method of image proposed to the present breast cancer detection named as confocal microwave imaging (CMI) bases on a synthetic aperture radar (SAR) [10, 11]. In our simulation, the numbers of antenna position correspond to $M = 19$. The calculation process is repeated at each antenna position. Although the incident wave and the reflected wave from the breast skin are much larger than that from the tumor, it is not difficult to distinguish those waves due to the difference of the time-of-flight.

To reconstruct the image, a point is focused. First, the distances between the focal point and each antenna position are determined and converted to the time delays. The reflected waves obtained by each antenna are summed up, and the square of this sum is assigned to the pixel value at the focal point. The intensity (I) of the pixel is assigned as

$$I(\vec{r}) = \left[\sum_{m=1}^{M} B_m(\tau_m(\vec{r}))\right]^2 \qquad (1)$$
$$\tau_m(\vec{r}) = 2\left|\vec{r} - \vec{r}_m\right| / v\Delta t$$

where B_m is the backscattered waveform at the mth antenna located at $\vec{r}_m$, and $\tau_m(\vec{r})$ is the time delay from the mth antenna to the synthetic focal point at $\vec{r}$. Here, the propagation velocity inside the breast is calculated by using the dielectric constant of the breast tissue.

We have performed the simulation using the chest section of numerical whole-body voxel human model of Japanese adult female developed by National Institute of Information and Communications Technology (NICT), Kitasato University, Keio University, and Tokyo Metropolitan University [12]. The model is 160.0 cm in height and 53.0 kg in weight, which is completed by using the MRI images of human body. It was shown that the tumor of 2-5 mm in diameter located at 2-3 cm depth from the skin can be detected by using the model.

B. Experimental Apparatus

The schematic of a USPR is shown in Fig. 3. A probe beam is an 8 V, 65 ps FWHM pulse. The FFT spectrum extends 8-10 GHz. The impulse is fed to an antenna. The reflected wave detected by an identical antenna is recorded by a high-speed sampling scope. The antennas attached to a rotational stage with a stepping motor are moved every 5 degree around the breast model from 0 to 180 degrees through the top. The reflected waves from the breast model are received at each antenna location, thus 37 reflected waves are provided. For the present experiment, we use a phantom model simulated for real breast biopsy (CRIS: model 051). The picture is shown in Fig. 3, which have a relative dielectric constant close to 20 and attenuation of 19 dB/cm at 8 GHz. The phantom skin layer is 55-mm higher, lying 20 mm below from the antenna elements. This distance provides a reasonable coverage of a model by an antenna radiation pattern. Dielectric materials with 6-9 mm in diameter used as tumors are located at around 10-25 mm depth from the top of the breast model.

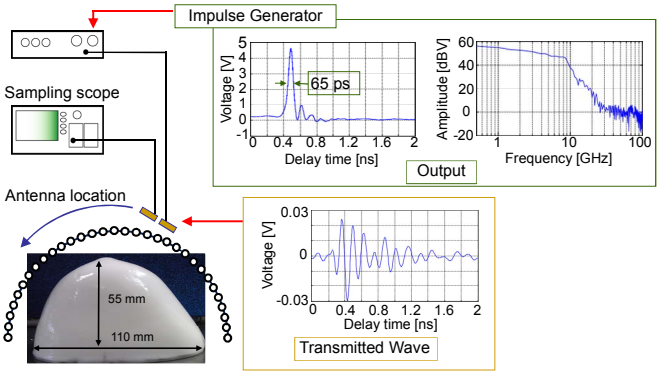

Fig. 3. Experimental apparatus of the USPR.

The antennas should efficiently focus the microwave signal towards the target and collect the back-scattered wave. A wideband antenna with unidirectional radiation pattern is required for the applications. The antenna should also be compact for easy installation, and the ease in fabrication of the arrays. The Vivaldi antenna is selected since it provides wideband characteristic with acceptable performance. The antenna was fabricated on 1.57 mm thick Taconic TLX substrate with dielectric constant of 2.7.

C. Experimental Results

The data contains additional undesired signals such as the antenna coupling, the reflections from the skin as well as the tumor response. They were preprocessed for background subtraction before using the focusing/image reconstruction algorithm. Teflon covers are used for background subtraction The primary aim of this process is to equalize or time-aligned the scattered response from tumors as received by antennas in different locations.

The results are shown in Fig. 4 for two different locations of tumor, 10 mm and 15 mm from the surface of the phantom together with a reconstructed image. The surface reflection levels are reduced by more than factor of 5 compared to our previous measurements.

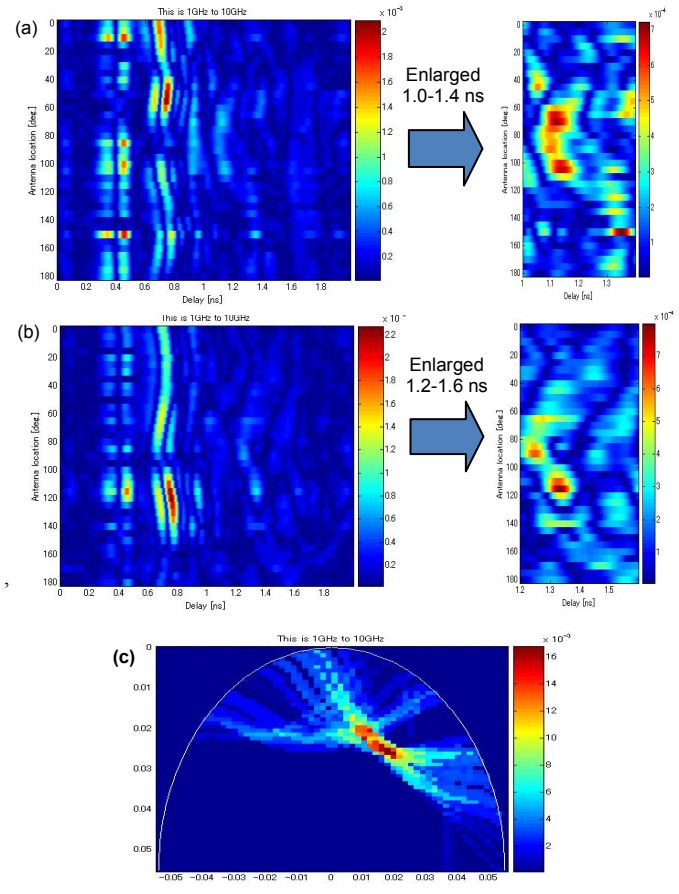

Fig. 4. Reflected wave from the position of (a) 10 mm and (b) 15 mm, and (c) image reconstruction of the object.

IV. Conclusions

Microwave reflectometry is a diagnostic tool that uses radar techniques. It has widely been used in magnetically confined plasmas, since it provides good spatial and temporal resolutions while requiring a single viewing chord. The combination of reflectometry and 1D/2D detector array thus gives 2D/3D profiles of plasma, which is called microwave imaging reflectometry (MIR). This MIR system has been applied to the LHD plasma. The feature of the system is the use of incident beam with 4 different frequencies and 2D detector array (horn mixer array). The MIR gives temporal and spatial characteristics of the MHD instability in LHD.

We have also performed the imaging diagnostics for breast cancer detection using a phantom model which is approximate to the actual breast tissue. It is effective to detect the breast cancer tumor by confocal microwave imaging using back-ground subtraction method to give better signal-to-noise ratio.

Acknowledgments

This work is partly supported by the Grant-in-Aid for Scientific Research, The Ministry of Eduaction. Science, Sports, and Culture (No. 16082205, No. 20360186 and No. 21246140), and Strategic Information and Communications R&D Promotion Programme (SCOPE), The Ministry of Internal Affairs and Communications (No. 121810001).

References

[1] C. Laviron, A. J. H. Donné *et al*., "Reflectometry techniques for density profile measurements on fusion plasmas," *Plasma Phys. Control. Fusion,* vol. 38, pp. 905-936, Jul. 1996.

[2] H. Park, C. C. Chang *et al*., "Recent advancements in microwave imaging plasma diagnostics," *Rev. Sci. Instrum*., vol. 74, pp. 4239-4261, Oct. 2003.

[3] M. Ignatenko, A. Mase *et al*., "Numerical study of microwave imaging reflectometry for measurements of density fluctuations in a tandem mirror plasma," Nucl. Fusion, vol. 46, pp. S760-S770, 2006.

[4] Y. Nagayama, D. Kuwahara *et al*., "Development of 3D microwave imaging reflectometry in LHD," *Rev. Sci. Instrum.,* vol. 83, 10E305, Oct. 2012.

[5] J. J. Xia, T. M. Habashy, and J. A. Kong, "Profile inversion in a cylindrically stratified lossy medium," Radio Sci., vol. 29, pp. 1131-1141, 1994.

[6] C. H. Jones, "Methods of breast imaging," Phys. Med. Biol., vol. 27, pp. 463-499, Apr. 1982.

[7] S. C. Hagness, A. Taflove, and J. E. Bridges, "Two-dimensional FDTD analysis of a pulsed microwave confocal system for breast cancer detection: fixed-focus and antenna-array sensors," *IEEE Trans. Biomed. Eng.,* vol. 45, pp. 1470-1479, Dec. 1998.

[8] Y. J. Kim, L. Jofre, F. D. Flaviis, and M. Q. Feng, "Microwave reflection tomographic array for damage detection of civil structures," *IEEE Trans. Microw. Theory Tech.*, vol. 51, pp. 3022-3032, Nov. 2003.

[9] A. Fhager, S. K. Padhi, and J. Howard, "3D Image Reconstruction in Microwave Tomography Using an Efficient FDTD Model," IEEE Antenna Wireless Propagation Lett., vol. 8, pp. 1353-1356, Aug. 2009.

[10] E. C. Fear, Xu Li *et al*., "Confocal microwave imaging for breast cancer ditection: localization of tumors in three dimensions," *IEEE Trans. Biomed. Eng.* vol. 49, pp. 812-822, Aug. 2002.

[11] M. Klemm, I. J. Craddock *et al*., "Radar-based breast cancer detection using a hemispherical antenna array–Experimental results," *IEEE Trans. Antennas Propag.* vol. 57, pp. 1692-1704, Jun. 2009.

[12] T. Nagaoka, S. Watanabe *et al*., "Development of realistic high-resolution whole-body voxel models of Japanese adult male and female of average height and weight, and application of models to radio-frequency electromagnetic-field dosimetry," *Phys. Med. Biol.* vol. 49, pp. 1-15, Jan. 2004